Vertical Structure and Turbulence in the Very Stable Boundary Layer

L. MAHRT

Department of Atmospheric Sciences, Oregon State University, Corvallis, OR 97331

(Manuscript received 11 February 1985, in final form 28 May 1985)

ABSTRACT

The structure of turbulence in a strongly stratified nocturnal boundary layer is studied using fast-response aircraft data collected under clear sky conditions with weak ambient flow. The principal source of turbulence is shear generation near the top of the surface inversion layer. This shear is induced by the development of surface flow which appears to be cold air drainage. The downward heat flux in the turbulent shear zone acts to warm the upper part of the inversion layer and is opposed by clear-air radiative cooling and advection of cold air.

The horizontal structure of the turbulence is studied using conditional means and other properties of the joint frequency distribution and analysis of the eigenvectors of the correlation matrix. Often, the turbulence exhibits statistical properties consistent with shear instability on horizontal scales near 300–400 m. Although modified by stratification, the main motions are turbulent-like with sharp horizontal boundaries and lead to net downward heat transport. The overturning also appears to lead to some buoyancy instability on somewhat smaller scales. The smaller scale turbulence is more three-dimensional but some influence of stratification is evident on horizontal scales even smaller than 100 m.

1. Introduction

Models of the stable boundary layer generally express the boundary layer depth and other characteristics in terms of surface fluxes and associated parameters such as the surface friction velocity and Obukhov length. These models appear to successfully approximate the weakly or moderately stratified boundary layers where the turbulence is more or less continuous and the strongest stratification may assume the form of a capping inversion (Nieuwstadt and Driedonks, 1979; Wittich and Roth, 1984). However, models based on surface fluxes poorly describe the very stable boundary layer (Arya, 1981).

Turbulence in the very stable boundary layer, as defined here, is generated intermittently by local shear and only indirectly related to any surface fluxes. As a result, the vertical structure of the very stable "boundary layer" may assume a variety of forms. To avoid introducing new terminology we must stretch the usual meaning of boundary layer and postpone refinement of semantics until the various regimes are better understood. We now briefly discuss two forms of the very stable boundary layer, each of which have appeared in previous studies.

a. Low-level wind maximum

A low-level wind maximum may develop near the top of the surface inversion layer due to inertial effects (Blackadar, 1957) and a variety of other mechanisms (see Mahrt, 1982 for a partial survey). If accelerations are only modest, fully-developed turbulence will not be maintained throughout the surface inversion layer. Then, significant turbulence seems to be confined mainly to the adjacent surface and near the wind maximum where shear extends into weak stratification above the surface inversion layer (Mahrt *et al.*, 1979). Clear-air radiative cooling is relatively important (Garratt and Brost, 1981) and may contribute to the extension of the inversion layer above surface-based turbulence (André and Mahrt, 1982).

b. Directional shear zone

In this case, directional shear near the top of the surface inversion layer generates turbulence. This directional shear may be induced by downslope drainage of cold air which occupies the inversion layer (Manins and Sawford, 1979; Garratt, 1982; Mahrt and Larsen, 1982; Yamada, 1983; Blumen, 1984). Turbulence also develops near the surface. However, most of the inversion layer between the surface based turbulence and the shear zone may remain nonturbulent.

These two types of stable boundary layers, as envisioned here, are idealized prototypes. Influences from both boundary layer prototypes may occur simultaneously as well as interact with other external influences such as terrain drag. Although poorly understood, the very stable boundary layer is of considerable practical interest since the weakness of the turbulent transport allows buildup of particulates and gases which are released at the surface. The suppression of turbulence can also lead to especially cold surface temperatures.

Here we will analyze fast-response data collected by

the NCAR Queen Air in a nocturnal surface inversion layer. These measurements were taken during a fair weather period in the Severe Environmental Storms and Mesoscale Experiment (SESAME) conducted in the state of Oklahoma in April and May of 1979. Aircraft slant soundings to within 15 m of the surface were implemented to provide repeated sampling of the vertical structure of the surface inversion layer and to provide information on spatial variability of such structure. Repeated horizontal flights were flown over the same track within and near the top of the surface inversion layer. The resulting data allow estimates of turbulence statistics at a given level.

Intermittent turbulence for this case is generated primarily by directional shear at the top of the surface inversion layer as in the second prototype boundary layer. The shear is induced by surface flow of cold air which is directed down the regional scale slope and is probably cold air drainage. Surface data from a network of portable automated stations located throughout Central Oklahoma indicate that surface winds were less than 2 m s^{-1} with considerable spatial variation of wind direction. These surface wind directions showed only a modest tendency to be directed down the local slope. The flow above the surface inversion was directed toward the north or northwest with a speed of a few meters per second. For the two remaining nights when the aircraft flew in the boundary layer, not analyzed here, winds were much stronger and significant turbulence was continuously maintained throughout the boundary layer.

Sections 3–5 will examine the vertical structure of the boundary layer as motivated above. The turbulence is found to be intermittent and mainly confined to the shear zone at the top of the surface inversion layer. Sections 6–7 examine properties of the turbulence itself. Previous analysis of turbulence in stratified atmospheric flow has been primarily limited to spectral decomposition. Conditional sampling, which has been frequently and successfully applied to study motions in the heated boundary layer does not seem very applicable to stratified turbulence where events are difficult to define. In some flow cases, organization by gravity waves provides a basis for compositing (Finnigan *et al.*, 1984). In this study, conditional mean distributions will reveal useful information on the multivariate relationships between temperature and the three wind components. Analysis of the eigenvectors of the correlation tensor will allow classification of motion types. Together these two approaches lead to inferences about the characteristics of the turbulence and indicate the extent of buoyancy oscillations, initial shear instability and more developed three-dimensional turbulence.

2. Data analysis

We analyze several horizontal aircraft legs and eleven slant soundings between 0530 and 0640 LST 5 May 1979. Sunrise occurred at approximately 0600 LST. However, changes in the surface inversion layer and overlying turbulence could not be detected until after 0700. Flights were aligned in the north–south direction and accumulated 84 000 data points during this period, each separated by a distance of approximately 4 m.

The instrumentation is as outlined in Wyngaard *et al.* (1978). Temperature measurements are somewhat tentative because thermal inertia of the thermistor housing reduces the high frequency response. We have adopted the correction procedure used in Wyngaard *et al.* (1978). The conclusions in this study are not significantly affected by the use of this correction which influences scales much smaller than the main transporting scale. Aircraft time was converted to distance using a constant aircraft speed of 80 m s^{-1} which leads to an overestimate of distance of 5–10% for some of the records.

After high-pass filtering with a cutoff wavelength of 500 m to partially remove gravity waves, the standard deviation of the vertical velocity in the patches of intermittent turbulence is usually about 10 cm s^{-1} with strongest vertical motions reaching about ½ m s^{-1}. These stronger motions dominate the structure of the turbulence examined in this study. For comparison, thermal updrafts average closer to 1 m s^{-1} in the middle of the strongly heated boundary layer although vertical motion fluctuations are much weaker between thermals and near the top and the bottom of the boundary layer (e.g., Lenschow and Stephens, 1980).

The standard deviation of the vertical velocity outside the turbulent patches is sometimes less than 1 cm s^{-1}. The spectral shapes of such weak signals do not exhibit expected features of instrument problems or instrumental noise. This suggests the measurement of some actual turbulence outside the turbulent patches in addition to any instrumental noise. These weak motions will not be analyzed here.

Horizontal aircraft flights provide direct information on horizontal structure without imposing Taylor's hypothesis. However, the choice of the horizontal length scale used to define the "turbulence" is a formidable problem, analogous to the problem of choice of time scale for analysis of time series. In stratified turbulence, a spectral gap between wave motions and "turbulence" is often not well-defined. This is partly due to overturning on scales that are only a factor 2 smaller than the smallest obvious gravity waves. The overturning also leads to sharp boundaries which distribute energy over the entire spectra and further obscures any separation of scales in spectral space. Since records are of finite length, restrictions on window width or number of lags is necessary for spectral decomposition. This further obscures any gap in spectral space. Thus any flux calculations will be sensitive to averaging length, detrending procedures and filtering. At the same time, flux calculations seem almost meaningless without high-pass filtering or alternative attempts to remove trend.

Additional Reynolds averaging terms associated with detrending, $\overline{w'\bar{\phi}}$ and $\overline{\bar{w}\phi'}$, do not vanish, where the overbar includes removal of trend and ϕ designates one of the wind components or temperature. In the present study, the extra Reynolds terms associated with the filtering were systematically about ⅓ of the main term $\overline{w'\phi'}$ and of same sign for the horizontal flights of width of 10–15 km but were sometimes as large as the main term for shorter records corresponding to turbulent patches of width of several kilometers. Clearly any flux calculations reported here must be considered as only order of magnitude estimates. A final sampling problem is that the net flux may be a smaller difference between turbulent gradient transfer and countergradient transport due to rebounding turbulent motions, or nonlinear waves as implied by the study of Finnigan *et al.* (1984).

The definition of turbulence and mean flow seems little affected by the ambiguity of coordinate system due to terrain variation. Slopes were typically about ½% or less on the scale of 5–10 km. On smaller scales, such slope values can be larger. The horizontal aircraft flights are flown at approximately constant height above ground although the pilot response to small scale terrain variations is not possible. When analyzing slant flights, we will use height above the local terrain surface which has been smoothed using a 200 m low-pass filter. The terrain height is computed as in Mahrt and Heald (1983).

a. Slant soundings

The eleven slant soundings are characterized by an aircraft ascent slope of about 1½%. Aircraft slant soundings allow estimation of the vertical structure with implicit horizontal averaging. However, several special problems with slant soundings must be considered. The first problem is contamination of the measured vertical velocity. Since the aircraft ascent slopes are $O(10^{-2})$ and vertical velocity fluctuations are only a few factors smaller than the magnitude of the horizontal fluctuations and only an order of magnitude smaller than the absolute horizontal velocity, direct contamination of the vertical velocity is unimportant for the present case even if the error in the estimated ascent rate was 100%.

With slant records, vertical mean structure may contaminate the computed horizontal turbulent structure and vice versa. Artificial fluctuations induced by the mean vertical structure can be estimated from the following order of magnitude argument

$$(\phi')_a \sim \frac{\partial\bar{\phi}}{\partial z} SL \qquad (1)$$

where $\partial\bar{\phi}/\partial z$ is the estimated true vertical gradient, S is the aircraft ascent slope and L the horizontal length scale which defines the computed turbulence. The relative error is of the order

$$\frac{(\phi')_a}{\sigma_\phi} \sim \frac{\partial\bar{\phi}}{\partial z} SL/\sigma_\phi \qquad (2)$$

where σ_ϕ is chosen to be the average standard deviation of the turbulent fluctuations as estimated from horizontal flights.

Mean gradients are chosen to be the average vertical gradients from 20–70 m as estimated from the composited soundings in Fig. (2) in Section 4. The vertical variation of mean vertical velocity is too small to measure. Table 1 lists the relative errors computed from (2) after applying three different high-pass filters. The L-value is chosen to be the filter wavelength in which case Table 1 becomes a measure of the upper bound for the errors.

The relative errors seem important but perhaps no more so than uncertainties of turbulence variance associated with the somewhat arbitrary choice of horizontal length scale. At the usual levels of the turbulence, the vertical gradient of horizontal momentum is larger than that used in Table 1 while the potential temperature gradient is usually smaller (Fig. 4, Section 3). Thus the potential importance of the errors for potential temperature is probably significantly less in the turbulence patches while the errors for horizontal momentum is greater than estimated in Table 1. Horizontal velocity fluctuations computed from slant aircraft soundings will therefore not be used.

The contamination of computed vertical velocity fluctuations is expected to be much smaller. Vertical velocity fluctuations are the same order of magnitude as horizontal velocity fluctuations but the vertical gradient of mean vertical velocity are orders of magnitude smaller than vertical gradient of mean horizontal velocity and should experience no sharp changes with height. Therefore, vertical velocity fluctuations will be used as an indicator of turbulence.

Comparison between turbulence statistics computed from horizontal and slant flights failed to yield any systematic differences for any of the variables as discussed briefly in Section 6. Nonetheless, only vertical velocity variance and the bulk vertical structure of the

TABLE 1. Estimation of errors for slant soundings where σ_ϕ is estimated from the horizontal flights, S = 1½%.

	$\partial\bar{\phi}/\partial z$	σ_ϕ	$(\phi')_a/\sigma_\phi$
	L = 200 m		
θ	3.4×10^{-2} K m^{-1}	0.13 K	0.78
u	1.0×10^{-2} s^{-1}	0.12 m s^{-1}	0.25
v	1.3×10^{-2} s^{-1}	0.10 m s^{-1}	0.39
	L = 500 m		
θ	3.4×10^{-2} K m^{-1}	0.15 K	1.70
u	1.0×10^{-2} s^{-1}	0.14 m s^{-1}	0.54
v	1.3×10^{-2} s^{-1}	0.12 m s^{-1}	0.81
	L = 5 km		
θ	3.4×10^{-2} K m^{-1}	0.37 K	6.89
u	1.0×10^{-2} s^{-1}	0.58 m s^{-1}	1.29
v	1.3×10^{-2} s^{-1}	0.47 m s^{-1}	2.07

heat flux will be evaluated from the slant flights. To minimize any temperature contamination problems, we choose L to be 200 m for analysis of slant soundings which may omit a significant portion of the transporting turbulence. Use of such values of the heat flux in this study will be compared first to values obtained from horizontal flights to help ensure at least the correct order of magnitude.

We must also consider the problem that low frequency horizontal fluctuations $\sigma_\phi(L)$ on horizontal scale L and larger will contaminate the computed vertical gradient of the mean flow. Since the sign of this error reverses randomly between soundings, slant soundings will be composited to reduce the role of such errors.

For purposes of defining vertical structure, each slant sounding is subdivided into record segments of horizontal length of 200 m corresponding to a change of vertical height above ground of about 3 m, although this value varies due to variations in local terrain slope and variations of ascent rate. The typical depth of a turbulent patch appears to be about 20 m.

The mean and fluctuation part of the flow are defined by computing a linear least-squares fit for each segment. This simple procedure yielded fluctuation variances which were generally a little larger than values obtained by low-pass filtering with a 4-pole Tangent-Butterworth filter with a wavelength cutoff of 200 m. However, in both cases, flux values were the same order of magnitude and exhibited the same qualitative vertical structure. Comparable results were obtained by detrending with least-squares cubic splines with nodal points every 200 m although the spline technique sometimes led to spurious oscillations. The average value of each variable and its variance are computed for each record segment. The slant soundings are composited and only limited use will be made of individual soundings by themselves. Composite profiles were computed by first interpolating to levels located every 10 m above the ground and then averaging over all of the soundings at each of the interpolation levels.

b. *Horizontal flights*

Inspection of the raw records and analysis of the correlation and covariance tensor (not reported here) indicate that internal gravity waves dominate variations on scales greater than 1 km while intermittent energetic turbulence appears to be confined mainly to scales less than 500 m although a complete scale separation probably does not occur. A partial merging of turbulence and gravity wave scales seems likely, a possibility noted by Caughey (1982). Certainly, the gravity waves are not as regular as in the recent study of Finnigan *et al.* (1984) and, undoubtedly, contribute to some of the high-pass variance. On the other hand, the motions at the 500 m scale are considerably more nonlinear and three-dimensional than motions on scales larger than one kilometer. A four-pole Tangent Butterworth filter with a cutoff value of 500 m was used to partition the flow.

Turbulent patches were generally characterized by sharp boundaries so that it was possible to extract segments of the record coinciding with such patches. The boundaries of these patches were not only obvious in terms of motion amplitude but also in terms of qualitative appearance. Therefore, the patches were defined by inspection. Only patches with $\sigma_w > 5$ cm s^{-1} were retained where σ_w is the standard deviation of the 500 m high-pass vertical velocity. For these turbulent patches, the vertical velocity fluctuations of the main transporting eddies are greater than 10 cm s^{-1}. Most of the turbulence observed here is a little weaker than the intermittent turbulence observed by Blumen (1984) near the top of a gravity flow.

Twenty-two patches of turbulence were identified with an average width of 4 km. The actual width of the patches could be greater since the aircraft may fly through the top or bottom of the patch if such boundaries are not horizontal. Thirteen patches of weaker turbulence with σ_w between 1 and 5 cm s^{-1} were also identified. An additional 12 patches of turbulence of various turbulence strength were located in the slant records. For the analyses and conclusions of this study, both of these additional classes of turbulence data possess various multivariate properties close to those of the 22 patches from horizontal flights where $\sigma_w > 5$ cm s^{-1}. Even though the properties of these three groups of data seem to be indistinguishable, we will analyze only statistics for the group of 22 patches that was observed from horizontal flights and contained the strongest turbulence.

In addition to statistics for individual patches, statistics representing the entire population of 22 patches were computed in three ways. In the first way, parameters were computed for each patch and then averaged over all of the patches. In a second approach, one large population of data was created by simply combining all of the patch records. Such statistics are generally strongly influenced by the most vigorous turbulence patches. In a third calculation, the variables are scaled by their standard deviation for each patch and then one large population of data is created. This approach essentially weights each patch equally. The statistics for the three approaches are qualitatively similar. Results will be reported here for the first approach, except that the joint frequency distributions of the total population can be constructed in a more general way by using the third approach.

3. Mixing events

We can construct examples of the vertical and horizontal structure of the flow and the preferred regions for development of turbulence by studying the two cross sections which could be constructed from the two undulating aircraft flights flown during the period of interest (Fig. 1). These undulating flight paths also

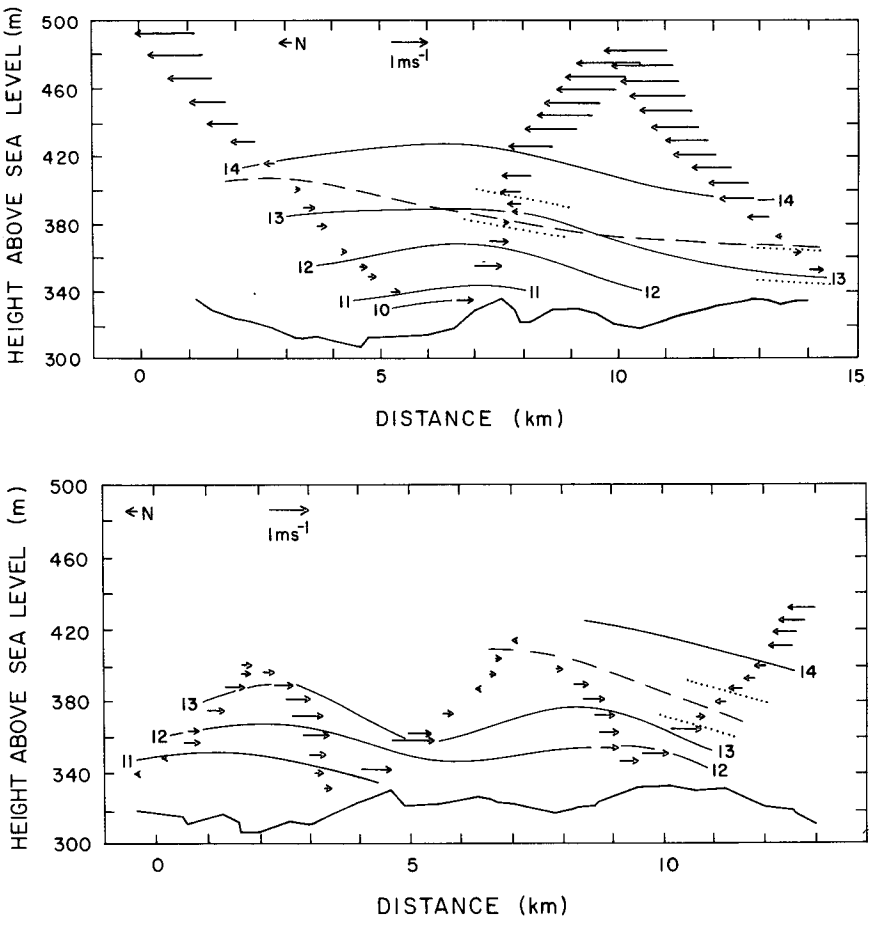

FIG. 1. Two cross sections of low-level airflow constructed from aircraft data taken with two similar undulating flight tracks (north is on the left). The lower solid line marks the terrain surface. Also shown are lines of constant potential temperature (°C, solid lines) and wind vectors indicating speed in the north–south direction. Dotted lines enclose regions of vertical velocity variance greater than 1 $cm^2\ s^{-2}$.

contribute to the sample of slant soundings analyzed in Section 4.

The cross sections show cold, strongly stratified, air near the surface flowing southeastward with a speed of typically one meter per second. Above this surface inversion layer, warm air is moving northward with a representative speed of 1 m s^{-1}. The cold surface air moving southeastward is usually approximately 50 m thick and tends to thin and become slightly warmer toward the southeast, implying cold air advection or subsidence. The southeastward direction would be consistent with drainage of cold air down the slope which prevails on a scale of several hundred kilometers.

The thickness of this cold airflow also varies locally and may even vanish, giving the impression of surges of cold air as previously observed by Geiger (1975), Doran and Horst (1981) and Mahrt and Larsen (1982). Of importance to this study is that the turbulence is intermittent and most often occurs at the transition between the southeastward moving cold air and northward moving warm air, as in the cross sections (Fig. 1). At this level the shear is significant and the stratification is weaker than in the underlying cold inversion layer. The air within the cold air layer in these examples contains very little turbulence. The flow immediately adjacent to the surface may be turbulent and perhaps directed down the local slope but it was not measured.

4. Vertical structure

Five of the eleven slant soundings show significant small-scale turbulent activity at the transition zone between the two airflows where the vertical velocity variance exceeds 15 $cm^2\ s^{-2}$. The remaining soundings contained little turbulence at any level. To form a statistical picture of the mean profiles and to reduce the influence of horizontal inhomogeneity occurring with individual soundings, we now study the composited soundings computed according to the procedures outlined in Section 2 and plotted in Fig. 2.

Since the level of the transition zone varies substantially from sounding to sounding, the maximum of the

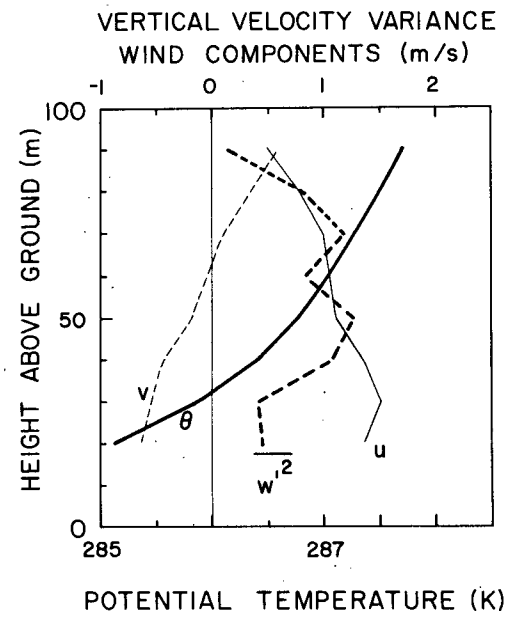

FIG. 2. Profiles composited from eleven aircraft soundings for potential temperature, southward flow (v), eastward flow (u), and vertical velocity variance which is expressed in 10^{-2} m^2 s^{-2} using the upper scale.

vertical velocity variance of the composited sounding is diffuse and poorly defined. Comparing the mean flow of the five cases with a turbulent transition zone with the six cases without turbulence indicates that turbulence is generated when significant southeastward flow develops near the surface (Fig. 3). This leads to large

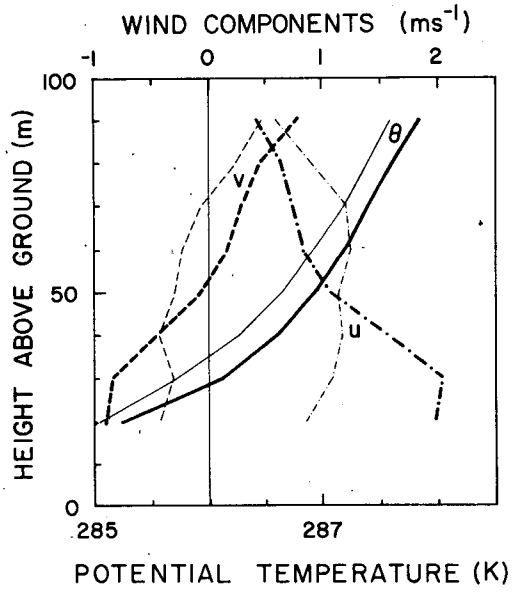

FIG. 3. Composited profiles for potential temperature (solid lines), northward flow (broken lines) and eastward flow (dashed-dotted lines) for the 5 soundings with significant turbulence (thicker lines) and the 6 soundings with little turbulence (thinner lines).

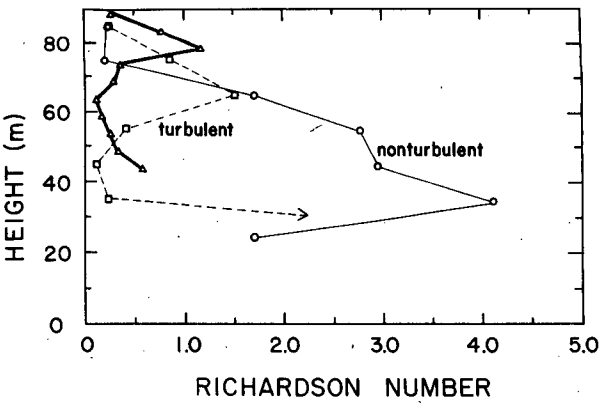

FIG. 4. The Richardson number computed from the composited profiles for the five soundings with significant turbulence (broken line) for these five soundings as a function of height relative to the level of maximum turbulence (thick solid) and for the six soundings with little turbulence (thin solid).

shear and relatively small Richardson number (<¼) near the top of the surface inversion layer as compared to the cases with little turbulent activity (Fig. 4) where the Richardson number was greater than three in this region. Of course, the minimum value of the Richardson decreases with increased resolution. For example, the bulk Richardson number between 20 and 70 m is approximately 1.3 for the turbulent class and about 9 for the nonturbulent class. This confirms the expectation that bulk Richardson number > 1, for example, does not rule out shear generation on smaller scales. For individual soundings, the relationship between turbulence and the Richardson number shows considerable scatter probably due to various sampling problems, as discussed in Section 2, and the possible phase lag between intermittent turbulence and mean shear as noted by Finnigan *et al.* (1984), and others.

The mean vertical variation of the patches is estimated by defining height relative to the level of maximum vertical velocity variance usually occurring near the center of the patch. Figures 4–6 show the profiles constructed by first interpolating variables to levels every 5 m above and below the level of maximum vertical velocity variance for each individual sounding. Values were then averaged for each of these levels. Compositing for the 5 slant soundings where significant turbulence activity occurred (Fig. 6) indicates that the thickness of the turbulent layers are about 15 or 20 m assuming that the aircraft did not systematically exit the side of the patch before crossing the top or bottom. The turbulent layers coincide with the top of the layer of strong shear which occurs in the transition between the cold southeastward flow and the overlying, warm, northward flow. A broad region of minimum stratification occurs near the top, and above the layer of turbulence. The significant turbulence extends downward into the upper part of the inversion layer where the shear is strongest. That is, the stratified side of the transition supports the largest shear without yielding to

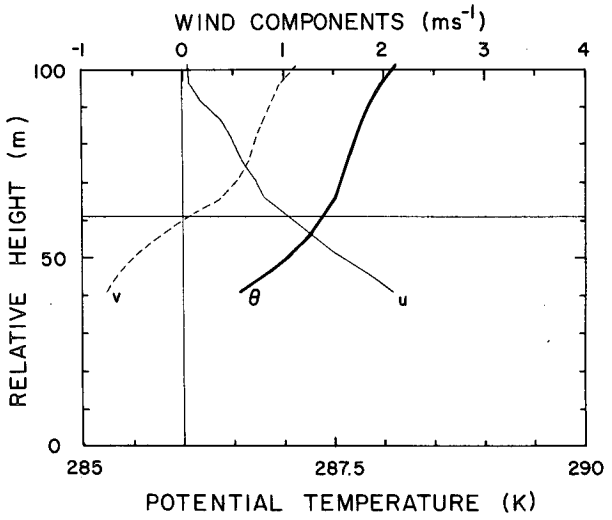

FIG. 5. Composited profiles of potential temperature (thick solid), northward flow (broken) and eastward flow (thin solid) for the five soundings with significant turbulence as a function of height relative to the level of maximum turbulence. The average value of this level is indicated by a thin horizontal line.

vigorous instability. This type of asymmetric shear zone is expected to be a common feature at the top of nocturnal surface inversions but has no close analogy with previous laboratory studies or theories of shear instability.

The strongest turbulence coincides with the minimum value of the Richardson number (Fig. 4) occurring at the bottom of the sublayer which is partially mixed in both potential temperature and momentum. On three of the five soundings with turbulence, a sharp inversion caps the sublayer of minimum stratification. This feature is partially eliminated by the compositing process. The development of mixed sublayers has been previously noted by Li *et al.* (1983) and others.

5. Heat budget

The significant downward heat flux at the top of the cold air layer decreases within the inversion layer and thus acts to warm the upper part of the inversion layer. The downward heat flux in the turbulent transition zone averages about 2×10^{-3} K m s^{-1}. Since the transition zone is significantly turbulent about half of the time, the time-averaged heat flux across the transition zone is about 10^{-3} K m s^{-1}. The downward heat flux computed from horizontal flights close to the average level of the turbulence averages about 2×10^{-3} K m s^{-1} using a 500 m filter. The latter estimate includes more of the turbulence and does not suffer from possible samplings associated with slant flights, as discussed in Section 2. This transported heat is presumably distributed slowly throughout the cold air layer by weak background turbulence and occasional intermittent turbulence whose variance was typically an order of magnitude smaller than that in the turbulent transition zone. The heat transport is also spread vertically by the "wandering" of the turbulent transition region within the layer between 35 and 65 m.

The eddy diffusivity for heat for the small scale turbulence is approximately 4 cm^2 s^{-1} in the turbulent transition zone and less than 1 cm^2 s^{-1} below this zone. This value is quite low partly because it accounts for regions of essentially no transport. Unfortunately, there are not enough cases to obtain a mean warming profile from the turbulent heat flux convergence with respect to absolute height above ground. The downward heat transport of 10^{-3} K m s^{-1} at the turbulent transition zone would lead to a warming rate of about 0.36 K h^{-1}, if distributed over a 10 m layer, and 0.07 K h^{-1}, if distributed over a 50 m layer, although all of the cooling rates could be in error by a factor of 2.

Cooling due to radiational flux divergence was estimated from the radiation model applied in André and Mahrt (1982) using temperature and moisture values averaged over 10 m layers. Temperature and moisture were extrapolated from 20 m to the surface by assuming linear temperature variation to an average surface air temperature of 7°C. This value is based on tethered balloon data and nearby Portable Automated Mesoscale surface data. Measurements of surface radiation temperature from the aircraft imply that the vertical temperature gradient near the surface must be

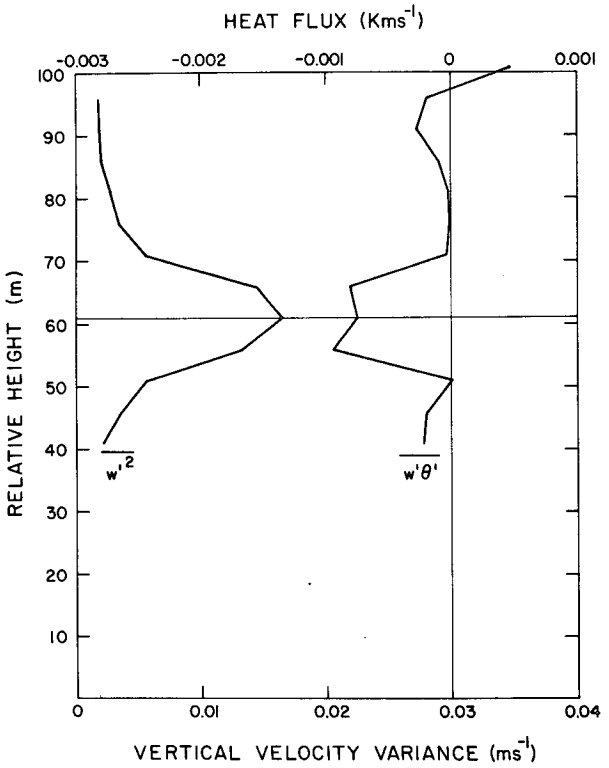

FIG. 6. Composited profiles of vertical velocity variance and heat flux for the five soundings with significant turbulence as a function of relative height (see text and Fig. 6).

quite variable and dependent on local terrain and surface conditions. Therefore, the radiation calculations near the surface may be in error. The estimated radiational cooling rate, averaged over all the soundings (Fig. 7), is largest in the layer between 25 and 50 m where it averages near 0.2 K h^{-1}. This appears to include much of the region of significant convergence of turbulent heat flux near the surface.

In fact, within accuracy of the calculations, the cooling due to radiation and the warming due to turbulence seem to be of comparable importance. Cold air advection and subsidence could also be important but cannot be estimated with sufficient reliability.

6. Horizontal structure of turbulence

Theories of wave and shear instabilities influence the way in which we interpret data collected in stratified turbulence. However, such theories are linear or quasi-linear. The patches here generally contain developed nonlinear turbulence due to the selection procedure. Some of the motions exhibit features consistent with shear-induced overturning but occur in an environment of significant ambient turbulence. The nonlinear nature of the flow for horizontal scales smaller than roughly ½ km is indicated by the importance of inertia terms compared to the buoyancy term. The nonlinear character is also implied by sharp horizontal variations at the edges of some turbulent motions as evident in the example in Fig. (8). This record also shows wavelike motion on scales of roughly 1 km and characteristic small scale pockets of very cold air. These features are common to most of the patches, and will be discussed further. Other features in the example in Fig. (8) are not necessarily observed in many of the other patches.

It also appears unlikely that the sharp variations in the present flow case can be efficiently represented by random superposition of the smooth eddies, as suggested by Townsend (1976) to explain behavior of the double velocity correlation function in laboratory turbulence. For the same reason, spectral decomposition is difficult to interpret. Such decomposition is shown in Fig. (9) to facilitate comparison with previous studies. Spectra and cospectra were computed for each of four aircraft legs flown in the layer of intermittent turbulence. Such legs are 10–15 km wide and approximately 60% occupied by turbulence, as defined by the criteria for the turbulent patches (Section 2).

The spectra indicate considerable activity at scales less than 100 m. The high wavenumber portion of the temperature spectra may be adversely influenced by the procedure to correct for thermal inertia. The horizontal velocity components show a broad peak centered at roughly 50 m. This energy is probably associated with small scale turbulence which appears to be quite prolific in the original records. This turbulence

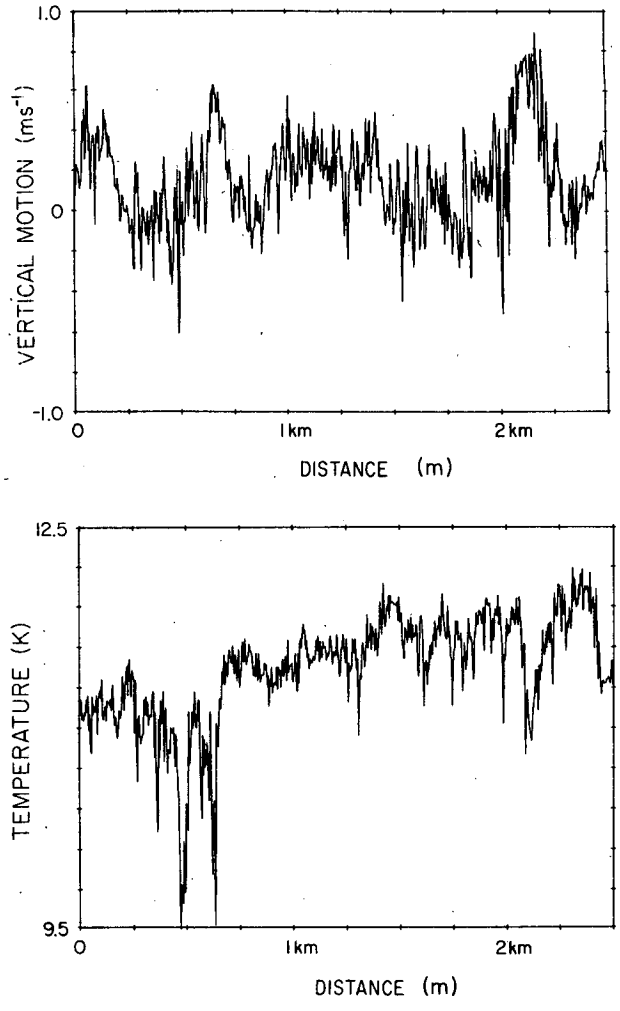

FIG. 8. Example of the temperature and vertical motion record for a vigorous turbulent patch. No detrending is applied.

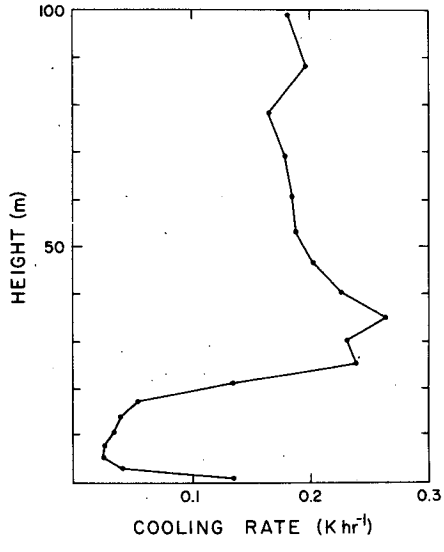

FIG. 7. The averaged profile of clear air radiational cooling rate. The near-surface cooling is expected to vary substantially due to horizontal inhomogeneity of surface temperature.

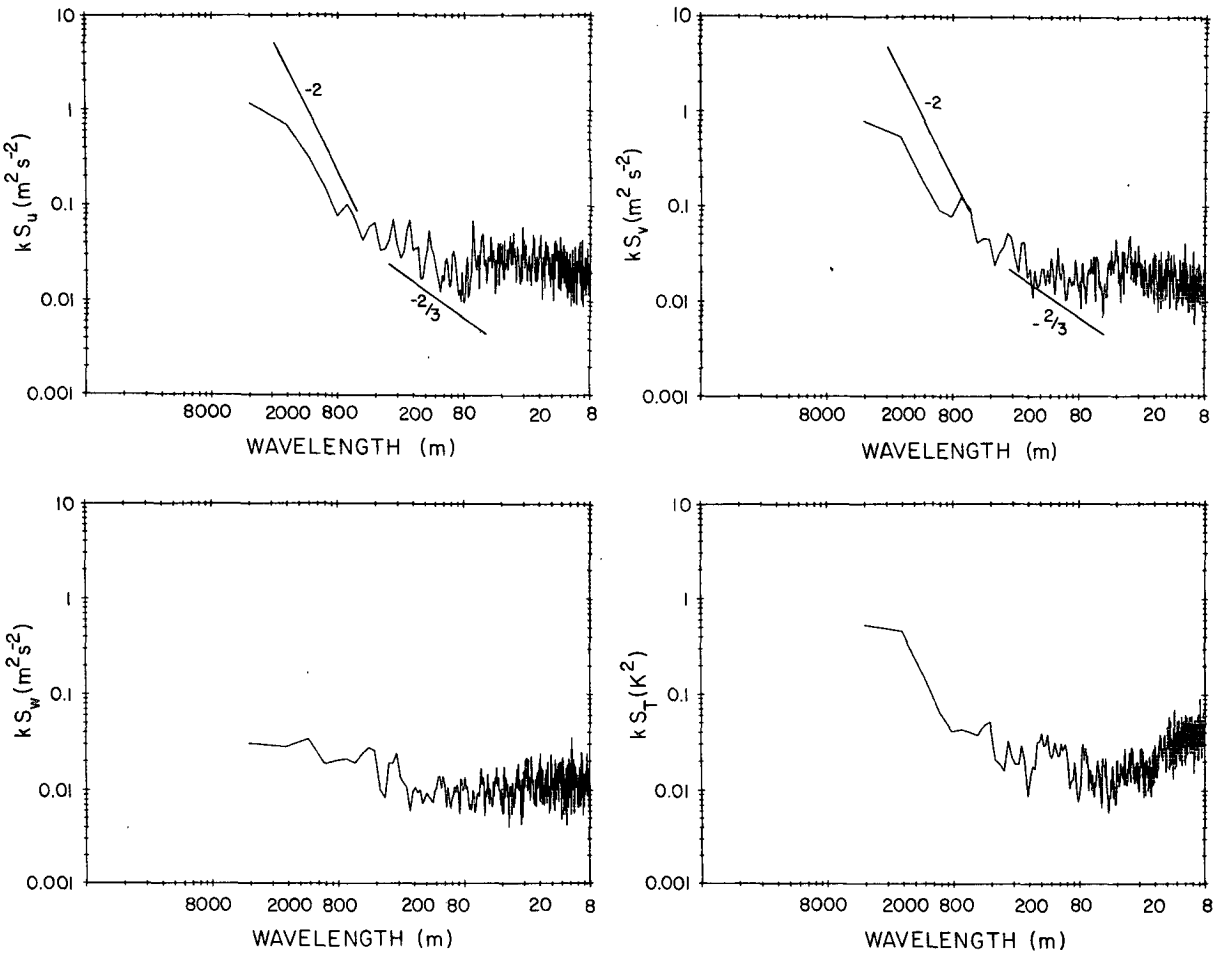

FIG. 9. Spectra averaged over the four horizontal legs containing substantial turbulence where S is the spectral density and k is the wavenumber. The coordinates are $\ln(k)S$ vs $\ln(k)$, although the abscissa is labeled in terms of wavelength.

leads to little measureable transport. The vertical motion variance at these small scales is typically 50% weaker than the variances for the horizontal components, suggesting that stratification exerts some restraining influence even on this small-scale turbulence. The spectra do not show an obvious inertial subrange which may be lost due to instrumental noise or resolution problems. These motions on scales less than 100 m exert little influence on the statistics which will be studied here.

The spectra of the velocity components also indicate spectral regions of significant activity on scales between 200 and 800 m which is superimposed on a general trend of increasing energy with increasing wavelength. The motions on these scales may lead to an inertial subrange which, however, would not be visible due to the activity peaking at scales less than 100 m. It is also possible that some of the energy generated at scales greater than 200 m is lost to gravity wave generation which would short-circuit establishment of an inertial subrange.

While wavelengths between 400 and 800 m lead to significant downward heat flux (Fig. 10), the quadrature exceeds the cospectra by roughly a factor of 2 in this spectral region, suggesting the presence of gravity wave motions. This ratio is about the same as observed by Zhou *et al.* (1985). Much of the variance on scales between 400 and 800 m in the present study could be contributed by wave motions especially at locations between turbulent patches. Cospectra of individual turbulent patches are vulnerable to significant sampling problems but generally show significant downward heat flux on scales somewhat smaller than 500 m. The physical interpretation of the spectra and cospectra is obscured by the fact that the Fourier modes, or even spectral bands, cannot be identified with specific turbulent phenomena. That is, the turbulent patches are not orders of magnitude wider than the width of the main eddies and the main eddies are not sinusoidal in nature. For this reason, this study will not rely significantly on spectral techniques.

Turbulent-like vertical motions with sharp horizontal boundaries appear on much of the original records usually on scales smaller than 500 m, suggesting that the motion is at least locally quite nonlinear. At the same time the vertical velocity variance on scales

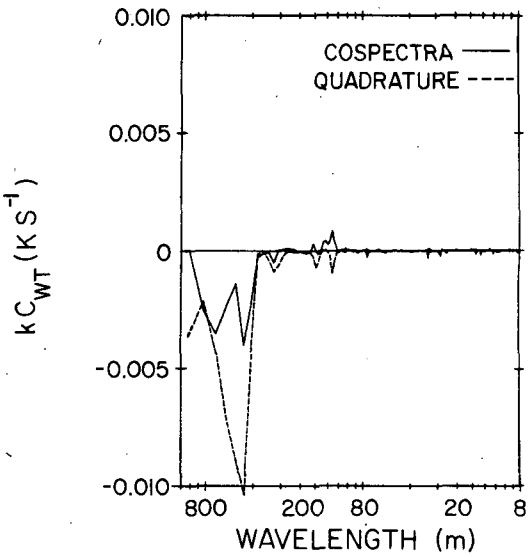

FIG. 10. Cospectra of the heat flux where C_{WT} is the cospectral density.

around 500 m is typically a factor of 2 or 3 smaller than the variance of the horizontal velocity components, indicating a significant influence of stratification. For comparison, this factor was more like 5–10 in the region of mixed waves and shear driven turbulence studied by Zhou *et al.* (1985).

Motions on scales larger than 1 km show increasing variance for horizontal velocity components and temperature but much less so for vertical motion. In fact, the vertical motion variance becomes 1–2 orders of magnitude weaker than that for horizontal components. Therefore, these larger scale motions are almost certainly not three-dimensional turbulence.

Analysis of autocorrelation and structure functions, not reported here, also indicates a difference in the nature of the flow between scales > 500 m and scales < approximately 500 m. For these reasons and recognition of sampling problems, we have chosen a cutoff filter of 500 m for the calculations in subsequent analyses. However, it is not possible to impose a clear cut distinction between turbulence and nonturbulent motions.

Inspection of the records also indicates that the qualitative appearance of turbulence varies from patch to patch. This variation may be due to sampling different stages of turbulence development and decay, and to sampling different levels with respect to the axis of the turbulent patch. The evolution of intermittent turbulence from initial shear instability to turbulence decay is thought to be a possible explanation of the variation of behavior of vertical velocity fluctuations near the top of cold air drainage in the study of Blumen (1984).

Here, we attempt to identify any recurring features of turbulence as revealed by analysis of the multivariate structure of correlation for the population of turbulent patches; we do not attempt to focus on possible local dominance of a single stage of development. Several statistical tools will be adopted to infer characteristics of the turbulence. In principle, we wish to study the simultaneous correlation between temperature and the three velocity components, in an effort to infer the structure of the turbulent motions. After high-pass filtering with a 500 m cutoff wavelength and removal of the mean, the variables are scaled by their standard deviation for each patch. The coordinate system was not rotated to the shear direction since the shear meanders somewhat. Since aircraft flights were nearly constant pressure, temperature is an adequate measure of buoyancy.

Characteristics of the joint relationship between variables for the turbulent patches are first studied by constructing the joint frequency distributions for the total population of observations (Fig. 11a) where variables were first scaled by the standard deviation of each patch. These joint frequency distributions indicate only a slight preference for downward heat flux and a modest preference for relative flow in the northeast–southwest direction. Also note the preference for very cold air with little vertical motion. The tendency for downward heat flux on the scale of hundreds of meters is diluted by the influence of the obiquitous smaller scale motions where the net heat flux is approximately zero. Individual turbulence patches sometimes show a strong preference for downward heat flux and occasionally significant upward heat flux.

The slight preference for downward heat flux for the entire population of turbulent patches is also evident from the contributions to the total covariance from different regions of the joint frequency distribution. Figure 11a arbitrarily shows the isoline (dashed) where the local sum, $\Sigma\ w'T'$ per unit area $\frac{1}{2}\sigma_w \cdot \frac{1}{2}\sigma_T$ equals 5% of the covariance summed over the entire population where σ_w and σ_T are standard deviations averaged over all of the turbulent patches. From the viewpoint of the joint frequency distribution for the entire population of data, the net heat flux seems to be a small difference between much larger opposing contributions.

Impressions formed from the joint frequency distribution are somewhat dependent on the choice of discretization of the distribution and choice of isoline values. Information about the joint frequency distribution and its variation between turbulence patches can be more quantitatively summarized by defining global properties of the joint frequency distribution. Such properties can be defined in a physical way by first posing the joint frequency distribution in polar coordinates (Mahrt and Paumier, 1984) somewhat analogous to construction of a wind rose. The particular version adopted in this study is explained in Fig. (12) where eight angle sectors are defined. For temperature and vertical motion, these sectors correspond to warm air with little vertical motion, rising warm air, rising motion with little temperature perturbation, and so forth.

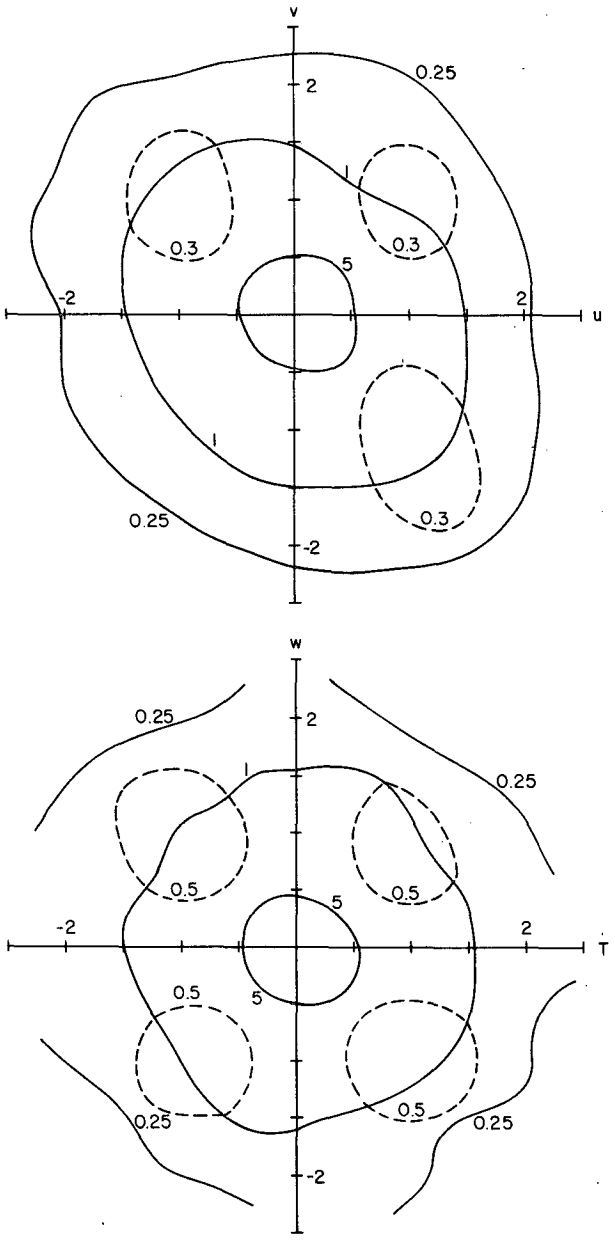

FIG. 11a. Joint frequency distribution of temperature and vertical motion. Thick solid lines indicate various percents of the total observations per unit area $\frac{1}{2}\sigma_T \cdot \frac{1}{2}\sigma_w$, the original resolution of the joint frequency distribution. Also shown is the isoline where $\Sigma\, w'T'$ per unit area $\frac{1}{2}\sigma_T \cdot \frac{1}{2}\sigma_w$, scaled by the total $\Sigma\, w'T'$, equals 5%. The analogous isolines are plotted on the joint frequency distribution for u and v except that the thin lines identify where $\Sigma\, u'v'$ per unit area $\frac{1}{2}\sigma_u \frac{1}{2}\sigma_v$ scaled by the total $\Sigma\, u'v'$, equals 3%.

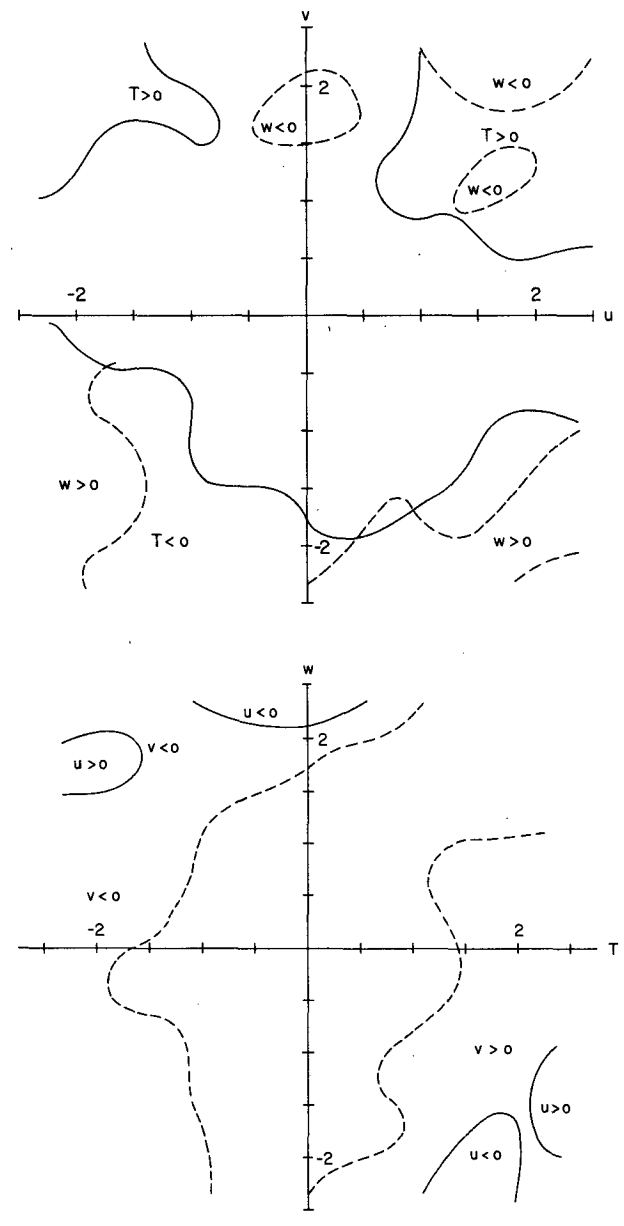

FIG. 11b. Conditional mean distributions of u (solid lines) and v (dashed lines) plotted on the w–T joint frequency distribution and conditional mean distribution for T (solid lines) and w (dashed lines) on the u–v joint frequency distribution. The isoline is plotted where the average value of the conditional variable exceeds 25% of its standard deviation.

For each sector of the joint frequency distribution of a given turbulence patch, we compute the number of occurrences N and the scaled joint variance (square of the amplitude)

$$r^2 = [\hat{T}^2 + \hat{W}^2] \tag{3}$$

where the caret denotes that the variable is scaled by the standard deviation. For a given polar angle, the flux is proportional to the number of observations and the joint variance r^2 (Mahrt and Paumier, 1984).

Large averaged variance indicates the prominence of significant events which create large fluctuations. For a given patch, we compute the average of the joint variance of the sector

$$\overline{r_j^2} \equiv \frac{1}{N_j} \sum_{i=1}^{n_i} r_{ij}^2 \tag{4}$$

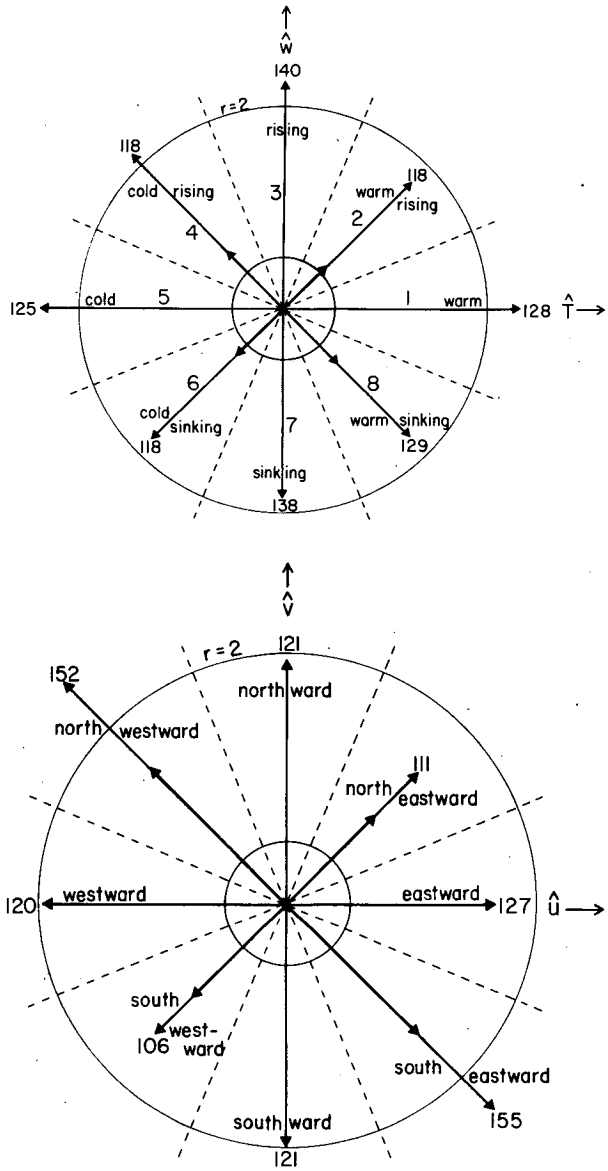

FIG. 12. Joint variance (r^2, thin solid) and covariance (thick solid) of $\hat{w}$–$\hat{T}$ and $\hat{u}$–$\hat{v}$ for each sector as averaged over the 22 turbulent patches. Solid outer circle denotes the average single distribution value of $r^2 = 2$. Inner solid line arbitrarily denotes where the average of the sector sum of the covariance, scaled by standard deviations, equals unity.

where j identifies the sector and i identifies an observation within the sector. The joint variance of a given sector is averaged over all of the turbulent patches and plotted in Fig. (12) along with the number of observations for each sector averaged over all of the patches. Finally, the scaled covariance for each sector

$$\sum_{i=1}^{N_j} \hat{w}\hat{T} \tag{5}$$

is averaged over all of the patches and plotted in Fig. (12, inner arrows).

The radius corresponding to the population average value of $r^2 = 2$ is plotted in Fig. (12) to assist the comparison of joint variance between patches. Relatively small differences in the joint variance between sectors can lead to significant correlation and production of net flux. Note that the odd numbered sectors corresponding to strong temperature perturbation and weak vertical motion, or large vertical motion and weak temperature perturbation generally earn larger joint variance than the even numbered sectors which contain both significant temperature and vertical motion amplitudes, as is also indicated by the joint frequency distribution (Fig. 11). Here pockets of especially cold air with weak vertical motion are prevalent. Warm air pockets are also found but less frequently, so that temperature is generally negatively skewed (Table 2). Since the turbulent patches normally occur at the top of the inversion layer, updrafts can pull rather cold air into the turbulent region. The overlying fluid is less stratified so that downdrafts produce smaller temperature fluctuations. There is some tendency for the largest negative temperature skewness to be generated by patches with the strongest turbulence energy (Table 2).

The occurrence of largest temperature fluctuations with weak vertical motion is consistent with parcel theory where the maximum temperature perturbation occurs just as the vertical motion vanishes and reverses direction. However, warm updrafts and cold downdrafts (sectors 2 and 6) lead to smaller covariance than the cold updrafts and warm downdrafts (sectors 4 and 8). As a result, the net heat flux is downward. Also note that a smaller number of high amplitude cold updrafts and a larger number of warm downdrafts lead to almost equal contributions to the downward heat flux. These characteristics are one of several clues that indicate that the dominant motions are not linear symmetric motions such as simple gravity waves but rather turbulentlike motions.

Analysis of the sector statistics for different pairs of the velocity components does not indicate a preference for low correlation (odd numbered) sectors in contrast to the distribution between temperature and vertical motion. These statistics (Fig. 12) and the joint frequency distributions (Fig. 11) indicate preference for sinking northwestward flow and rising southeastward flow as would be predicted by parcel theory, although the influence of pressure fluctuations is thought to be important. Rising southward surges are stronger than sinking northward velocity fluctuations and velocity fluctuations in the north–south direction are better developed and higher correlated with vertical motion than fluctuations in the east–west direction. This feature is discussed in the analysis below.

Further insight is revealed by constructing the conditional mean distribution (as recently applied by Grossman, 1984). Such averages are plotted in Fig. 11b for the population of turbulent patches. Largest values of the conditional means generally occur in the corners of the joint frequency distribution where the values of

TABLE 2. Statistics for individual turbulent patches.

Patch number	Standard deviation u (m s^{-1})	v (m s^{-1})	w (m s^{-1})	T (m s^{-1})	Skewness u	v	w	T	Correlation wT	uw	vw	uv	uT	vT
1	0.27	0.26	0.16	0.17	0.02	−0.20	0.04	−0.16	0.14	−0.16	−0.33	0.23	−0.12	−0.22
2	0.06	0.06	0.06	0.14	−1.79	−0.36	0.17	−0.56	−0.24	−0.14	−0.07	0.01	0.10	0.22
3	0.11	0.13	0.07	0.22	−0.11	−0.41	−0.05	−0.48	−0.13	−0.46	−0.04	−0.14	−0.01	0.47
4	0.13	0.17	0.08	0.23	−0.08	−0.42	0.19	−1.07	−0.07	0.03	0.08	−0.22	0.20	0.56
5	0.10	0.07	0.06	0.20	−0.65	0.65	−0.16	−0.37	−0.02	−0.22	0.09	−0.01	−0.10	−0.29
6	0.17	0.13	0.10	0.21	−0.43	−0.43	0.08	−0.57	0.09	0.38	−0.09	−0.08	0.48	0.43
7	0.28	0.18	0.16	0.21	−0.57	−1.22	0.04	0.20	−0.08	0.24	−0.11	−0.19	0.32	0.06
8	0.08	0.05	0.07	0.11	−0.31	0.15	0.08	−0.16	−0.07	0.04	0.09	0.12	−0.25	0.03
9	0.10	0.07	0.06	0.11	0.10	0.18	0.12	−0.08	−0.05	0.02	−0.02	−0.23	−0.20	0.29
10	0.23	0.20	0.12	0.15	0.54	−0.59	−0.24	−1.03	0.05	0.17	−0.18	−0.55	−0.42	0.22
11	0.33	0.25	0.19	0.25	0.04	−0.30	−0.21	−1.45	−0.15	0.24	−0.30	−0.37	−0.44	0.40
12	0.09	0.08	0.05	0.09	0.09	0.53	0.13	0.58	0.04	0.21	−0.13	−0.40	−0.28	0.20
13	0.16	0.13	0.06	0.10	−0.20	0.19	−0.09	−0.01	−0.04	0.09	−0.14	−0.59	−0.46	0.38
14	0.23	0.15	0.11	0.11	0.34	0.40	0.74	−0.10	−0.21	0.25	−0.32	−0.65	−0.65	0.63
15	0.05	0.07	0.05	0.11	−0.11	−0.90	0.35	1.68	0.18	−0.09	0.18	−0.30	−0.11	0.38
16	0.09	0.08	0.06	0.07	−0.31	0.23	−0.20	0.32	0.07	0.24	−0.12	−0.34	−0.01	−0.19
17	0.13	0.12	0.07	0.09	−0.47	0.80	0.17	−0.19	0.06	0.14	−0.24	−0.51	−0.28	0.03
18	0.07	0.07	0.06	0.07	0.69	−0.20	0.19	−0.57	−0.08	−0.01	−0.15	−0.15	−0.01	0.08
19	0.13	0.11	0.05	0.16	1.10	−1.31	0.69	0.95	−0.19	−0.09	−0.07	−0.60	0.26	−0.18
20	0.07	0.06	0.05	0.20	0.14	0.35	0.38	0.21	0.22	−0.05	0.03	−0.43	−0.05	0.18
21	0.11	0.07	0.09	0.10	−0.58	0.42	3.91	1.91	−0.17	−0.13	0.04	−0.40	0.28	−0.36
22	0.15	0.18	0.14	0.17	−0.04	0.08	0.35	0.42	−0.12	0.32	−0.37	−0.47	−0.46	0.57
Avg	0.14	0.12	0.09	0.15	−0.12	−0.11	0.30	−0.02	−0.04	0.05	−0.10	−0.29	−0.10	0.18

the two variables defining the coordinate system are also largest. The conditional mean distributions for the joint frequency distribution of temperature and vertical motion indicate the expected prominence of rising, cold, southeastward flow and sinking, warm, northwestward flow. The relationship between strong southward velocity fluctuations and very cold air is particularly well-defined. This relationship is evident in all of the combinations of the conditional mean distributions. It may be that such cold southward fluctuations occur during a surge in the general downslope flow. Such surges were suggested by Fig. (1). The weaker involvement of the east–west flow component may be associated with disruption of the larger scale terrain slope by rougher terrain and several low mountain peaks located a few tens of kilometers west of the flight track or may be due to influences of cold air drainage down the gently sloped valleys whose axes were roughly oriented in an east–west direction.

7. Motion types

Additional combinations of joint frequency distributions and conditional mean distributions do not contain significant new information owing to some redundancy between distributions and are therefore not shown. Although the above conditional averages reveal the average relationship between the four variables, such an analysis does not imply much about the nature of the motions leading to such statistics and cannot resolve situations where a given variable is locally important in determining the correlation structure but may assume opposing roles in different spatial regions. The resulting reversal of signs leads to cancellation in the conditional averaging process and corresponding loss of potentially important information.

This spatial variation can be included by determining the eigenvectors of the correlation matrix. Such eigenvectors transform the original observational vectors into principal components (e.g., Timm, 1975). Using the notation of Wallace and Dickinson (1972)

$$z_i(g) = \sum_{j=1}^{4} e_{ij} u_j(y). \tag{6}$$

Four principal components z_i are generated which are linear combinations of $u_j(y)$, the four original variables consisting of temperature and the three velocity components. Principal components (or empirical orthogonal functions) have been applied to analysis of the correlation tensor for shear driven turbulence by Payne and Lumley (1967). Discussion of the general technique and application to meteorological examples can be found in Kutzbach (1967) and Wallace and Dickinson (1972).

The eigenvectors of the correlation matrix e_{ij} essentially describe a transformation from the four-dimensional coordinate system defined by temperature and the three velocity components to a rotated coordinate system where each new coordinate is a linear combination of temperature and the three velocity components. We have also defined the arguments of the observational vector to represent different spatial positions, in order to define horizontal structure of the main

eddies. This analysis becomes physically quite complex and will not be reported here.

The first eigenvector explains a maximum amount of variance of the original four variables; the second eigenvector explains the maximum amount of the remaining variance, and so forth. Each of the four components of the eigenvector represent the relative importance and sign of the influence of each of the four original variables. The eigenvectors can then be classified according to the combination of signs of its components. Noting that multiplying the entire eigenvector by minus one corresponds to the same eigenvector, eight independent combinations of signs are possible. These combinations and physical identification are listed in Table 3. This physical identification describes aspects of "statistical" eddies. That is, the determination of the eigenvectors merely maximizes variance-explained which might be accomplished by assuming characteristics which lie somewhere between two or more prominent types of motions.

Nonetheless, certain eigenvector types are consistent with the geometry of known idealized eddies (Fig. 13). For example, simple gradient transfer is represented by eigenvector Ia (Table 3) while shear driven vorticies, as shown in Turner (1973) and Koop and Browand (1979) would lead to the succession of eigenvectors involving Ia, Ib, IIa and IIb. Two examples are shown at the bottom of Fig. (13). Buoyancy oscillations translated by their initial horizontal momentum correspond to eigenvector Ia followed by IIb. Pressure fluctuations may lead to development of significant flow perpendicular to the plane containing the shear and thus eigenvectors Ic, Id, IIc, IId. The importance of these four eigenvectors indicate the degree of three-dimensionality of the flow.

A given data set corresponding to a turbulence patch is completely described by four eigenvectors. The eigenvector corresponding to complete gradient transfer of heat and both momentum components is far more important than the other eigenvectors (Table 4) as might be anticipated from the previous conditional averaging on the joint frequency distributions. These motions correspond to cold, rising, southeastward flow

TABLE 3. Classes of eigenvector combinations.

Circulation type	Sign of coefficient			
	T	u	v	w
I. Downward heat flux				
a. Gradient transfer	+	−	+	−
b. Horizontal flow reversed	+	+	−	−
c. Cross-flow (v reversed)	+	−	−	−
d. Cross-flow (u reversed)	+	+	+	−
II. Upward heat flux				
a. Gradient momentum transport	+	+	−	+
b. Horizontal flow reversed	+	−	+	+
c. Cross-flow (v reversed)	+	+	+	+
d. Cross-flow (u reversed)	+	−	−	+

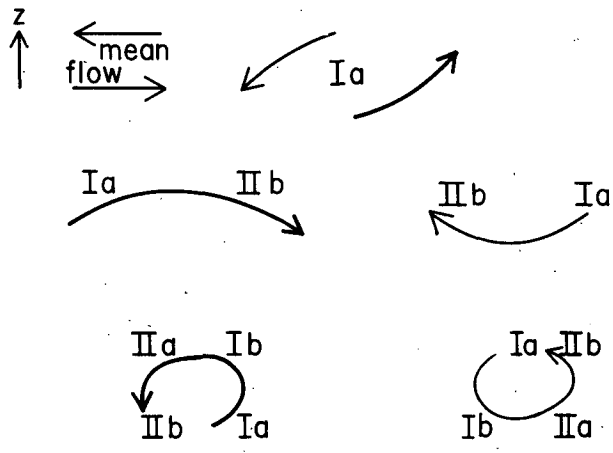

FIG. 13. Plausible geometric depiction of the main eigenvectors. Positively buoyant air is indicated by thin lines; negatively buoyant by thick lines.

and warm, sinking, northwestward flow. Table 4 lists the number of cases where a given eigenvector type explains more than 30% of the variance of a given turbulent patch. These eigenvectors usually include only the largest eigenvector of each turbulent patch. Although these eigenvectors were found to be highly significant using the usual tests (e.g., Harris, 1975), the assumptions and situations described by such tests have minimal meaning for the present application. Table 4 also summarizes results for all of the eigenvectors that explained more than 20% of the variance which always included the second most important eigenvector. Finally, Table 4 lists the percentage of the variance explained by each eigenvector averaged over all of the turbulent patches.

Complete gradient transfer (eigenvector Ia) is the largest eigenvector for about half of the turbulent patches. Although by far the most important, this eigenvector explains, on the average, only about ¼ of the total variance of the patches (Table 4). The failure of a single eigenvector persistently to explain a majority of the variance probably reflects the turbulent nature of the flow where a variety of motions coexist. Some of the variance not explained by eigenvector Ia, can be described by assuming equal distribution over all of the remaining types of motion, suggesting a random portion of the flow as would occur with fully turbulent motion. No motion type, other than complete gradient transfer, is persistently a dominant factor. The broader class of motions leading to downward heat flux with any type of momentum transport include the most important motion type for about 80% of the turbulent patches and explains a little more than 60% the total variance. Motions corresponding to upward heat flux counter to the mean gradient, only occasionally dominate a turbulent patch.

Noting that eigenvector Ib is the second most important mode and that eigenvectors IIa and IIb are of comparable importance suggests a conceptual model

TABLE 4. Percentage variance explained (pve) for the 22 turbulent patches and totals for all motions leading to upward heat flux (up) and downward heat flux (down).

	Eigenvector									
	Down				Up					
	Ia	Ib	Ic	Id	IIa	IIb	IIc	IId	Down	Up
Number of patches pve > 30%	11	4	1	3	2	3	0	0	19	5
Number of patches pve > 20%	13	7	4	5	8	8	2	6	29	24
Average pve	26	16	9	12	12	11	5	9	63	37

Average coefficients of the eigenvectors.

Eigenvector	*T*	*U*	*V*	*W*
Ia	0.46	0.45	0.56	0.37
Ib	0.38	0.55	0.37	0.44
Ic	0.55	0.45	0.36	0.37
Id	0.51	0.46	0.46	0.40
IIa	0.39	0.38	0.37	0.56
IIb	0.43	0.36	0.30	0.66
IIc	0.37	0.62	0.39	0.43
IId	0.51	0.13	0.11	0.80

of shear driven overturning (Fig. 13). Simple buoyancy oscillation would not explain the importance of modes Ib and IIa, while simple gravity wave instability with no shear would not explain the dominance of eigenvector Ia.

Adopting a conceptual model of shear-driven overturning (Fig. 13) for purposes of discussion, Table 4 indicates that after the initial stage (Ia), each of the subsequent stage of overturning explains less variance. As a result, the initial stages of downward heat flux lead to greater transport than the subsequent stages of upward heat flux. Apparently as the overturning proceeds, ambient turbulence distorts and interferes with overturning progress.

As the overturning approaches the 180° stage, the circulation may partially break down due to local thermodynamic instability. Local thermodynamic instability resulting from shear-driven overturning and the subsequent upward buoyancy flux associated with secondary turbulent motions have been observed in laboratory turbulence by Thorpe (1973), Koop and Browand (1979) and others. Upward heat due to secondary rebounding motions can also be inferred from turbulence in stratified laboratory flows where mean shear is not present. In the immediate region where the laboratory turbulence is generated, strong downward buoyancy flux is generated. As some of the displaced fluid accelerates back toward the buoyancy equilibrium level, the buoyancy flux decreases and may even locally reverse to small net upward buoyancy flux downstream from the generation region, as observed by Stillinger *et al.*, 1983. They suggest that the region of vanishing buoyancy flux may be associated with a transition from stratified turbulence to internal wave motions rather than buoyancy instability. Gravity wave activity is consistent with the relatively large quadrature at scales greater than 400 m (Fig. 10) and the wavelike activity at such scales suggested by inspection of the records outside regions of turbulence.

In contrast to the wave mechanism, local buoyancy generation of turbulence would imply increased activity on smaller spatial scales compared to the initial overturning scale. The occurrence of upward heat flux due to secondary buoyancy instabilities is consistent with the occurrence of small upward heat flux on smaller wavelengths between 100 and 200 m in the cospectra for some of the individual horizontal legs and patches. A small peak of upward heat flux also appears at smaller scales in the composited cospectra (Fig. 10) although the composited slant soundings indicated net downward heat transport at such scales.

Also note that the percentage variance explained by motions leading to upward heat flux is more distributed between various eigenvector types compared to motions causing downward heat flux. This suggests that the upward heat flux is caused by motions whose velocity field is more random. Spectral decomposition of the eigenmodes (not shown) similarly indicate that the more important eigenvectors Ia and Ib corresponding to downward heat flux are associated with larger scales compared to the scales of the eigenvectors corresponding to upward heat flux. Zhou *et al.* (1985) also observed upward heat flux at scales smaller than the spectral region of dominant downward flux for a case of turbulence in stratified flow above a shallow convective mixed layer.

The smaller scale upward heat flux suggests the occurrence of secondary buoyancy instabilities due to the

overturning and/or interaction with the smaller scale turbulence. Upward heat flux due to completion of the overturning or simple rebounding of displaced fluid acts to reduce the net downward heat flux on the scale of the overturning but could not by itself explain the upward heat flux on smaller scales. The smaller scale upward heat flux may also be related to mechanisms other than buoyancy instability such as smaller reverse eddies due to shear between updrafts and downdrafts of the main overturning eddies.

Horizontal motion perpendicular to the mean shear (eigenvectors Ic–d, IIc–d) explains about ⅓ of the total variance and may occasionally dominate individual turbulent patches indicating significant three-dimensionality. This estimate may be in error if some of the variance explained by these eigenvectors is due to meandering of the mean shear vector if such meandering is not considered to be turbulence. The slant records indicate significant variation of the u-component of mean shear. Fluctuations of u in general show erratic relationship with the other variables. Also, note that the averaged coefficients of eigenvector IId are small for the horizontal wind components (Table 4) implying that this eigenvector is more an indicator of upward heat flux with weak fluctuation of the horizontal motion. Nonetheless, much of the variance of eigenvectors Ic–d and IIc–d is probably due to motions perpendicular to the shear plane and caused by secondary shear and buoyancy instability and turbulent pressure fluctuations.

While linear shear instability theory usually predicts predominance of flow variance in the plane containing the mean shear, some specific shear instabilities quickly lead to significant energy for motions perpendicular to the mean shear (e.g., Corcos and Lin, 1984). This possibility, together with the occurrence of a partial spectral gap between the transporting motions on the scale near 500 m and small scale turbulence, suggests that some of the turbulence is young without a well-developed inertial subrange.

The foregoing results and inspection of the records for each patch confirm that the dominant motions are not likely described by a single eddy model of overturning. The degree of three-dimensionality and the value of the heat flux and other quantities vary significantly from patch to patch. While a single eddy model cannot describe the main turbulent motions of the various patches, repeated similar spatial structure do seem to occasionally dominate a single turbulence patch, perhaps due to common stage of turbulent development and orientation of the aircraft trace with respect to the main eddies within the patch.

8. Conclusions and discussion

The foregoing results indicate that the usual simple models of the structure of the stable boundary layer do not adequately describe the vertical structure of the very stable case. In this case, turbulence is generated mainly by shear at the transition between the surface flow and the overlying synoptic flow. This transition generally occurs near the top of the surface inversion layer and sometimes leads to partially mixed layers embedded within the upper part of the inversion layer.

Turbulence is weak below the shear zone, which favors buildup of contaminants as well as cold nocturnal surface temperatures. Quantitative flux estimates are difficult to interpret since they are contaminated with sampling problems aggravated by the intermittency of the flux. However, the various computational methods employed here all indicate important downward heat flux generated by the shear at the top of the cold air flow.

Since the downward heat flux is a maximum at the boundary layer top, turbulent transport leads to warming of the boundary layer as in the study of Manins and Sawford (1979) and Finnigan *et al.* (1984). This contrasts with the usual conceptual model of the nocturnal boundary layer where turbulent transport leads to cooling of the air. Here the warming due to downward turbulent heat transport is opposed by clear-air radiational cooling and possibly cold-air advection by the downslope flow. This heat balance describes the observations of the surface inversion layer at the end of the night. The rapid initial cooling of the nocturnal boundary layer at the beginning of the evening may be quite different.

The nature of the turbulence in this study is significantly influenced by the rapid decrease of stratification with height. For example, the temperature fluctuations at the top of the inversion are negatively skewed with a tail toward cold values. This feature explains some of the relationship between temperature and momentum structure. The temperature and horizontal velocity statistics are also influenced by surges of cold air which could be due to cold air drainage.

Much of the turbulence can be described by simultaneous gradient transfer of temperature and both horizontal momentum components. This appears to be the first phase of shear-induced overturning. Motions corresponding to subsequent phases of shear-induced overturning also seem important although they explain sequentially less variance and are somewhat more random, three-dimensional and smaller scale. The latter stages are characterized by upward heat flux which reduces the net downward flux resulting from initial overturning. This upward heat flux appears to be partly due to small scale buoyancy instability resulting from the overturning. While the most energetic transporting motions exhibit features consistent with shear-driven overturning, gravity waves appear to influence the statistics computed in this study.

The present study, together with some of the studies cited in the Introduction, indicates that the nocturnal boundary layer assumes a variety of vertical structures. Under conditions of clear skies and light ambient wind, the vertical structure appears to vary spatially over short distances in response to variations of terrain and surface

conditions. In large-scale and regional models of the atmosphere, these variations become subgrid scale variance. The transport by cold air drainage circulations, which was considered as advection in this study, would also contribute to the subgrid scale variance and vertical flux in larger scale models. There appears to be no reasonable way to include such flux suggesting that formulations of the very stable boundary layer in large scale models might as well be simple.

The foregoing study has also estimated various errors resulting from use of aircraft slant flights. For the data used here, errors in the vertical velocity fluctuations are unimportant. Errors in vertical heat fluxes are more important but these appear to be small compared to the more general problem of choosing a length scale to define the turbulence and compared to errors due to neglect of extra Reynolds terms resulting from detrending procedures.

Acknowledgments. I am grateful for the extensive computational assistance of James Paumier and Wayne Gibson and the timely and detailed comments of the reviewers. The radiation calculations were performed by Pierre Lacarrere and Jean-Claude André. This material is based upon work supported by the Meteorology Program of the National Science Foundation under Grant ATM-8306141. Important acknowledgment is made to the National Center for Atmospheric Research, which is sponsored by the National Science Foundation, for use of the Queen Air and for part of the computing time used in this research.

REFERENCES

André, J. C., and L. Mahrt, 1982: The nocturnal surface inversion and influence of clear-air radiative cooling. *J. Atmos. Sci.*, **39**, 864–878.

Arya, S. P. S., 1981: Parameterizing the height of the stable atmospheric boundary layer. *J. Appl. Meteor.*, **20**, 1192–1202.

Blackadar, A. K., 1957: Boundary layer wind maxima and their significance for the growth of nocturnal inversions. *Bull. Amer. Meteor. Soc.*, **38**, 283–290.

Blumen, W., 1984: An observational study of instability and turbulence in night-time drainage winds. *Bound.-Layer Meteor.*, **28**, 245–269.

Caughey, S. J., 1982: Observed characteristics of the atmospheric boundary layer. *Atmospheric Turbulence and Air Pollution Modelling*, Reidel, 107–158.

——, J. C. Wyngaard and J. C. Kaimal, 1979: Turbulence in the evolving stable boundary layer. *J. Atmos. Sci.*, **36**, 1041–1052.

Corcos, G. M., and S. J. Lin, 1984: The mixing layer: deterministic models of a turbulent flow. Part 2. The origin of the three dimensional motion. *J. Fluid Mech.*, **139**, 67–95.

Doran, J. C., and T. W. Horst, 1981: Velocity and temperature oscillations in drainage winds. *J. Appl. Meteor.*, **20**, 361–364.

Finnigan, J. J., F. Einaudi and D. Fua, 1984: The interaction between an internal gravity wave and turbulence in the stably stratified nocturnal boundary layer. *J. Atmos. Sci.*, **41**, 2409–2436.

Garratt, J. R., 1982: Observations in the nocturnal boundary layer. *Bound.-Layer Meteor.*, **22**, 21–48.

——, and R. A. Brost, 1981: Radiative cooling effects within and above the nocturnal boundary layer. *J. Atmos. Sci.*, **38**, 2730–2746.

Geiger, R., 1975: *The Climate Near the Ground*, Harvard University Press, 611 pp.

Grossman, R. L., 1984: Bivariate conditional sampling of moisture flux over a tropical ocean. *J. Atmos. Sci.*, **41**, 3238–3254.

Harris, R. J., 1975: *A Primer of Multivariate Statistics*, Academic Press, 332 pp.

Koop, C. G., and F. K. Browand, 1979: Instability and turbulence in a stratified fluid with shear. Part I, *J. Fluid Mech.*, **93**, 135–159.

Kutzbach, J. E., 1967: Empirical eigenvectors of sea level pressure, surface temperature and precipitation complexes over North America. *J. Appl. Meteor.*, **6**, 791–802.

Lenschow, D. H., and P. L. Stephens, 1980: The role of thermals in the convective boundary layer. *Bound.-Layer Meteor.*, **19**, 507–532.

Li, X-S., J. E. Gaynor and J. C. Kaimal, 1983: A study of multiple stable layers in the nocturnal lower atmosphere. *Bound.-Layer Meteor.*, **26**, 157–168.

Mahrt, L., 1982: Momentum balance of gravity flows. *J. Atmos. Sci.*, **39**, 2701–2711.

——, and S. Larsen, 1982: Small scale drainage front. *Tellus*, **34**, 579–587.

——, and R. C. Heald, 1983: Nocturnal surface temperature distribution as remotely sensed from low-flying aircraft. *Agric. Meteor.* **28**, 99–107.

——, and J. Paumier, 1984: Heat transport in the atmospheric boundary layer. *J. Atmos. Sci.*, **41**, 3061–3075.

——, R. C. Heald, D. H. Lenschow, B. B. Stankov and I. Troen, 1979: An observational study of the structure of the nocturnal boundary layer. *Bound.-Layer Meteor.*, **17**, 247–264.

Manins, P. C., and B. L. Sawford, 1979: Katabatic winds: A field case study. *Quart. J. Roy. Meteor. Soc.*, **105**, 1011–1025.

Nieuwstadt, F. T. M., and A. G. M. Driedonks, 1979: The nocturnal boundary layer: A case study compared with model calculations. *J. Appl. Meteor.*, **18**, 1397–1405.

Payne, F. R., and J. L. Lumley, 1967: Large eddy structure of the turbulent wake behind a circular cylinder. *Phys. Fluids (Suppl.)*, S194–S196.

Stillinger, D. C., K. N. Helland and C. W. Van Atta, 1983: Experiments on the transition of homogeneous turbulence to internal waves in a stratified fluid. *J. Fluid Mech.*, **131**, pp. 91–122.

Thorpe, S. A., 1973: Turbulence in stably stratified fluids: a review of laboratory experiments. *Bound.-Layer Meteor.*, **5**, 95–119.

Timm, N. H., 1975: *Multivariate Analysis*, Brooks/Cole Publishing, 689 pp.

Townsend, A. A., 1976: *The Structure of Turbulent Shear Flow*, Cambridge University Press, 429 pp.

Turner, J. S., 1973: *Buoyancy Effects in Fluids*, Cambridge University Press, 367 pp.

Wallace, J. M., and R. E. Dickinson, 1972: Empirical orthogonal representation of time series in the frequency domain. Part I, theoretical considerations. *J. Atmos. Sci.* **11**, 887–900.

Wittich, K. P., and R. Roth, 1984: A case study of nocturnal wind and temperature profiles over the inhomogeneous terrain of Northern Germany with some considerations of turbulent fluxes. *Bound.-Layer Meteor.*, **28**, 169–186.

Wyngaard, J. C., W. T. Pennell, D. H. Lenschow and M. A. LeMone, 1978: The temperature-humidity covariance budget in the convective boundary layer. *J. Atmos. Sci.*, **35**, 47–58.

Yamada, 1983: Simulations of nocturnal drainage flows by a Q^2L turbulence closure model. *J. Atmos. Sci.*, **40**, 91–106.

Zhou, Ming Yu, D. H. Lenschow, J. C. Kaimal and B. B. Stankov, 1985: Wave and turbulence structure in a shallow baroclinic convective boundary layer and overlying inversion. *J. Atmos. Sci.*, **42**, 47–57.